Three-Phase Transformerless Shunt Active Power Filter with Reduced Switch Count for Harmonic Compensation in Grid-Connected Applications

Wajahat Ullah Khan Tareen, *Member, IEEE,* and Saad Mekhielf, *Senior Member, IEEE*

***Abstract*—Shunt active power filter is the preeminent solution against nonlinear loads, current harmonics and power quality problems. APF topologies for harmonic compensation use numerous high-power rating components and are therefore disadvantageous. Hybrid topologies combining low-power rating APF with passive filters are used to reduce the power rating of voltage source inverter. Hybrid APF topologies for high-power rating systems use a transformer with large numbers of passive components. In this paper, a novel four-switch two-leg VSI topology for a three-phase SAPF is proposed for reducing the system cost and size. The proposed topology comprises a two-arm bridge structure, four switches, coupling inductors, and sets of LC PFs. The third leg of the three-phase VSI is removed by eliminating the set of power switching devices, thereby directly connecting the phase with the negative terminals of the dc-link capacitor. The proposed topology enhances the harmonic compensation capability and provides complete reactive power compensation compared with conventional APF topologies. The new experimental prototype is tested in the laboratory to verify the results in terms of total harmonic distortion, balanced supply current, and harmonic compensation, following the IEEE-519 standard.**

***Index Terms*—Harmonics, hybrid topology, nonlinear load, power quality (PQ), Transformerless inverter, Grid-connected system.**

I. Introduction

The proliferation of nonlinear characteristic loads generates voltage and current harmonics in the power distribution system. At the distribution level, the current harmonics generate problems, such as power quality, reactive power, transformer losses, voltage harmonics, and harmonic resonance. These problems can be mitigated by using active solutions, including shunt active power filters (SAPFs) and hybrid APFs (HAPFs). These filters are connected in series or shunt coupling consisting of passive and active components [1, 2]. These filters also limit the flow of current harmonics into the power distribution system, in accordance with strict harmonic standards, such as IEEE 519 [3].

A typical APF consists of a voltage source inverter (VSI) of a three-leg bridge structure with a dc-link capacitor. Conventional APF topologies require a matching transformer and a large number of active switching devices, such as the insulated gate bipolar transistor (IGBT); thus, these topologies are disadvantageous [4]. These considerations result in heavy weight and costly system and are therefore undesirable.

In [5-7], a transformer-less three-phase pure SAPF is integrated with diode rectifier nonlinear load. The SAPF is connected through the coupling inductor at the point of common coupling (PCC) in the shunt position with the power distribution system. This topology is composed of a six-switch three-leg full-bridge VSI with a dc-link capacitor and coupling inductors. The designed ac inductors are implemented to shape the input current and compensate the current harmonics.

A transformer-less HAPF for overcoming the limitation of high-power rating inverters is presented in [8]. This topology consists of a three-phase six-switch bridge inverter connected in series with a passive filter (PF). The low-power rating inverter compensates the current harmonics at the PCC flowing into the utility source and improves the filtering characteristic of the series LC PF.

On the other hand, a reduced switch count transformer-less HAPF is illustrated in [9, 10]. The new design uses four switches to test the two-leg bridge inverter by connecting the removed leg with the negative terminal of the dc-bus. Besides reducing cost, it offers less complex structure, high reliable filtering compensation, and controlled balanced dc-link voltage.

In the present paper, a transformer-less SAPF topology based on a four-switch two-leg structure is presented. Unlike other existing topologies, the new circuit is derived from the six-switch full-bridge inverter. The new model enhances harmonic filtering and reactive power compensation

Manuscript received March 19, 2017; revised May 23, 2017; accepted July 04, 2017. Date of publication XXXX; date of current version XXXX. The authors would like to acknowledge the financial support from the University of Malaya, Malaysia, through the Postgraduate Research Grant (PPP) PG338-2016A and the Ministry of Higher Education of Malaysia through the Fundamental Research Grant Scheme (FRGS) FP014-2014A and Malaysian International Scholarship (MIS). Recommended for publication by XXXX.

The authors are with the Power Electronics and Renewable Energy Research Laboratory, Department of Electrical Engineering, Faculty of Engineering, University of Malaya, Kuala Lumpur 50603, Malaysia. (E-mail: wajahattareen@gmail.com; saad@um.edu.my).

Color versions of one or more of the figures in this paper are available online at http://ieeexplore.ieee.org.

Digital Object Identifier XX.XXXX/TPEL.201X.XXXXXX

This article has been accepted for publication in a future issue of this journal, but has not been fully edited. Content may change prior to final publication. Citation information: DOI 10.1109/TPEL.2017.2728602, IEEE Transactions on Power Electronics

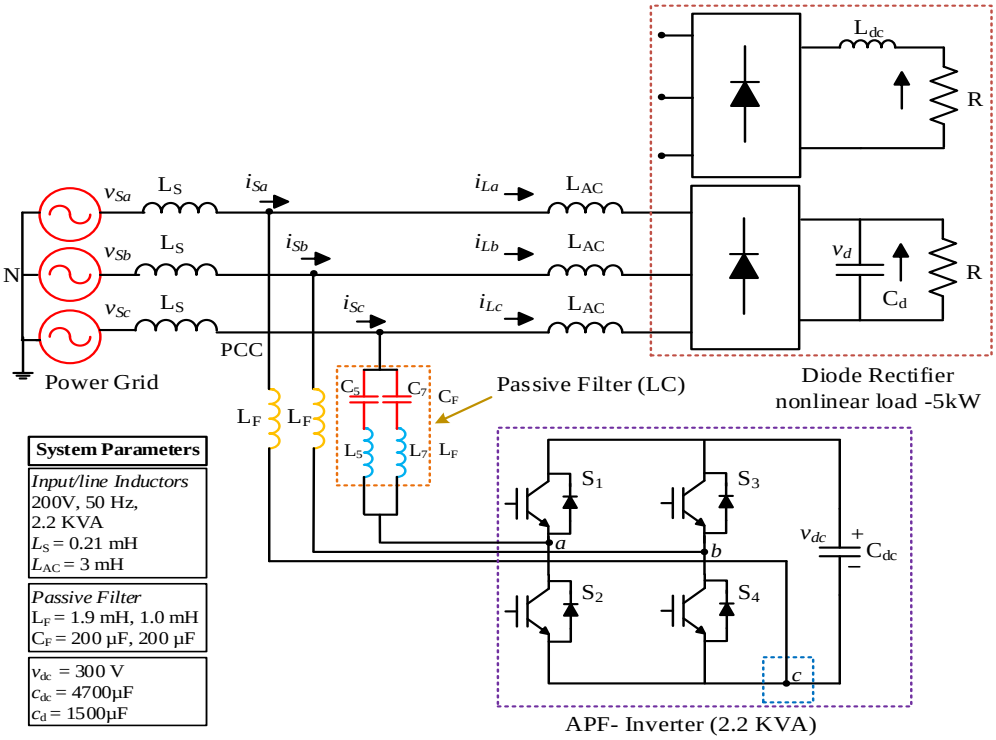

Fig. 1. Proposed transformerless APF system

comparable to conventional full-bridge topologies.

The proposed design mainly aims to provide superior compensation capability and less complex structure without increasing the number of power switching devices for three-phase applications. The series ac-coupling inductors overcome the fixed reactive power compensation by limiting the use of PFs. The new topology provides superior overall performance as compare to the dc-bus midpoint connection configuration in terms of harmonic compensation capability owing to the balanced current and voltage. Therefore, less complex structure and straightforward connection between the transmission line and the terminal of the dc-bus reduce the constraint of voltage balancing across the dc-link capacitor. This configuration also eliminates the need of extra controller and transformer in between the LC PF and the filter inverter for preventing magnetic saturation. As a result, the design configuration presents less cost, volumetric size, and lightweight structure. The rest of the paper is organized as follows. The proposed system configuration and system analysis are described in Section II. The system analysis is subdivided into proposed four-switch two-leg inverter analysis, PF analysis and design, reactive power compensation and filtering characteristic. Section III reports the overall control system. Section IV and Section V presents the simulation and experimental results. Section VI elaborates the conclusions.

II. PROPOSED FOUR-SWITCH TWO-LEG VSI-SAPF

In this paper, a novel four-switch two-leg VSI topology for a three-phase SAPF is proposed for reducing the system cost and size. The proposed SAPF is composed of the three-phase two-leg bridge version of the four-switch inverter, as shown in Fig. 1. It comprises a two-arm bridge structure, four switches, coupling inductors and sets of LC PFs. The adopted modulation strategy in this study is the sinusoidal PWM (SPWM) for a proper switching scheme. The carrier signal is compared with the comparators with single modification to pattern the reference signals [10].

The third leg of the three-phase VSI is removed by eliminating the set of power switching devices, thereby directly connecting the phase with the negative terminals of the dc-link capacitor. The elimination of single phase-leg generates the dc-link voltage imbalance or voltage fluctuations issues [11]. Therefore, this problem can be solved by connecting the removed leg terminal with the negative terminal of the dc-bus PWM-VSI to stop the unbalance charging of the dc-link capacitors [9]. Furthermore, to stop the flow of decoupling power ripples, the ac film capacitor stores the power ripples [12], to provide the balanced output currents and voltages. Unlike other existing topologies, the new circuit is derived from the six-switch full-bridge inverter presented in [7]. The new model enhances harmonic filtering and reactive power compensation comparable to conventional full-bridge topologies.

The proposed system mainly aims to provide superior compensation capability and less complex structure without increasing the number of power switching devices for three-phase applications. The series ac coupling inductors overcome the fixed reactive power compensation by the LC PF, the two ac inductors are coupled to the two phases of VSI. The reduced leg terminal is linked through the sets of LC filters, including the inductor and capacitor set. In the reduced leg, the direct connection between the utility power line and the dc-link terminal divides the dc voltage and shifts it to the

output voltage of the power converter. Therefore, the PFs are used to reduce the power and voltage requirement against the utility fundamental component at the output of the inverter (*phase c*). In addition, the inductors are used as a filter against the switching ripple generated from the switching converter. The capacitor of the PF provides the fundamental reactive power demand to the load and reduces the dc current circulation and also dc voltage. However, it presents poor performance at low-order harmonic frequencies, except at the tuned 7th harmonic frequency. Therefore, the two sets of LC filters are tuned at the 5th and 7th harmonic frequencies to compensate the current harmonics and improve the filtering characteristic.

A. Proposed four-switch two-leg inverter analysis

For simplicity of analysis, source voltage $(V_{sx} = V_{xf} = V_{pcc})$ and load voltage (V_x) are considered as sinusoidal waveforms $(V_x = V_{pcc})$, without the harmonic components $(V_{sx} = V_x)$. The coupling passive power component is represented by $(Z_{shF} = Z_{PPFf} = Z_{Fabc})$ which comprises a series resistor, an inductor and a capacitor. The inductance is a short circuit path owing to the low rated value as demonstrated in Fig. 2.

Fig. 2 illustrates the single-phase fundamental equivalent reference circuit from the filter inverter fundamental voltage phasor $(V_{inv-shxf})$ to the output, where "*f*" shows the fundamental frequency component.

$$V_{inv-shxf} = V_x - Z_{shf}.\mathrm{I}_{cxFf} \tag{1}$$

where the fundamental compensating current phasor (I_{cxFf}) is divided into real and reactive components as

$$I_{cxFf} = I_{cxFfp} + jI_{cxFfq} \tag{2}$$

where the subscripts "*p*" and "*q*" represent the active and reactive components. I_{cxFfp} is the fundamental active current component that compensates the loss and dc-link voltage control, and I_{cxFfq} is the fundamental reactive current component that compensate the reactive power in the system load. Thus, expression (1) can be simplified as follows

$$V_{inv-shxf} = V_{inv-sxfp} + jV_{inv-sxfq} \tag{3}$$

$$V_{inv-sxfp} = V_x + I_{inv-sxfq}.X_{Ff} \tag{4}$$

$$V_{inv-sxfq} = -I_{inv-sxfp}.X_{Ff}$$

As shown in expression (2) and (4), the fundamental compensating active current (I_{cxFfp}) and the reactive compensating current (I_{cFxfq}) are extracted into

$$V_{cFfp} = -\frac{I_{inv-sxfq}}{X_{Ff}} \tag{5}$$

$$V_{cFfq} = -\frac{I_{inv-sxfp} - V_x}{X_{Ff}} \tag{6}$$

The value of the reactive dc current (i_{qDC}) is controlled in the quadrature axis and the value of the direct axis is set to zero to compensate the fundamental reactive power and protect the APF from being damaged. In the steady state, the active fundamental current (I_{cFxfp}) is insufficiently small

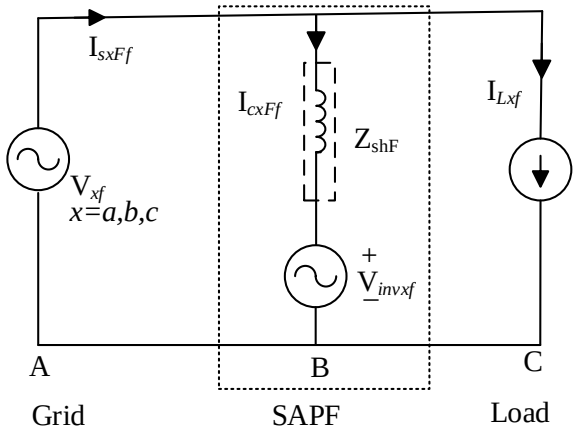

Fig. 2. Fundamental equivalent circuit of the proposed APF system.

$(I_{cFxfp} \approx 0)$; thus, this current is generated by the inverter to maintain the constant dc-link voltage level. Therefore, with constant dc voltage level and modulation index around (m≈1), the ratio between the DC-link voltage and the load voltage (V_x) is expressed in expression (7), where $(V_{inv-sxf})$ is the inverter fundamental RMS voltage.

$$R_{V_{dc}} = \pm\frac{V_{inv-sxf}}{V_x} = \pm\frac{v_{dc}}{2\sqrt{2}V_x} \tag{7}$$

B. PF design and analysis

The design stages of the proposed transformerless APF consists of two parts; 1) the design of active filter inverter and 2) the design of the passive filter. Generally, each PFs consists of inductors and capacitors sets connected in series with the active inverter. The PFs are installed in the single removed leg of the power VSI to provide reactive power compensation and absorbing harmonic currents from a diode rectifier load.

In design process, the value of the (L_F), and (C_F) parameters are identified, referring to the harmonic content of the three phase diode rectifier load. Thus, the three-phase diode rectifier load produces few harmonics at the 11th and 13th harmonic frequencies. Therefore, the LC filters are tuned at the most dominant order 5th and 7th harmonic frequencies in between the grid phase and negative terminal of the dc-link capacitors. The low value filter inductance makes the APF system unstable and increases the switching ripples [13]. Therefore, the filter inductance value (L_F) should be ten times larger than the supply inductance (L_S) in order to acquire an attenuation ratio of 10%. To achieve the lower impedance (550 Hz and 650 Hz) of the PF, it is tuned to 350 Hz than the PF tuned to 250 Hz. Likewise, the PF is tuned to 7th dominant harmonic frequency in order to reduces the bulky weight than a 5th harmonic filter for the filter capacitor (C_F) [14].

The selection criteria of the LC passive filter design depends upon two factors; 1) The larger value of the capacitance will makes the PF bulky and results in a high reactive current. 2) And the lower value of inductance increases the switching ripples produces from the inverter. The L_F and C_F parameters are calculated as presented in study [15]. In demand to PFs design specification and define criteria, a less expensive and cost effect 2.0 kVAR passive filter at 200V

utility line voltage tuned around 360 Hz is tested and installed in the switch reduced leg of the hybrid APF system [16]. The calculated values of the LC PF filter is fabricated following the design specification, as listed in Table III. The resonance frequency should be chosen rightfully between the tuning frequency range in 200 and 550 Hz, because without the APF inverter the harmonic amplifying occur in the frequency range of 200–340 Hz.

1) Circuit schematic of the proposed APF: The circuit schematic of the proposed APF model is shown in Fig. 3. The high voltage rating of the model helps in reducing the device conduction and switch losses to nearly zero. The exiting of the high amount of current results in high winding loss; however, the current peak is low because of being tuned to the 5th and 7th harmonic frequencies, thereby resulting in low inductor losses. However, the switch losses increases under the high switching frequency operation in the conventional six switch topology. Therefore, in the proposed novel four switch topology, the number of switches can be effectively decreased, resulting no problem under this condition. The effective filtering characteristic depends on the equivalent impedance of the PF (Z_F = Z_{Fabc}). However, the PF is tested at low impedance to avoid the harmonic amplifying phenomena. The harmonic resonance in the PF [17] causes wide range frequency tuning. Therefore, the use of PF is limited to the single phase of the power converter compared with other topologies. In other words, the capacitor of the LC filter stops the dc-link voltage component and provides the required stability margin caused by the utility voltage.

The through connection of the utility phase line to the negative terminal reduces the dc-link voltage and shifts half of the dc-link voltage to the output voltage at the power converter; therefore, this converter is composed of switching ripple, dc-link, and amplified modulation components [10], as mention in expression (8).

$$\frac{v_{dc}}{2} + k_{con} v_m(t) + v_{swr}(t) \tag{8}$$

where v_{dc} is the dc-link voltage, $v_m(t)$ is the modulation signal, k_{con} is the gain of the power converter, and $v_{swr}(t)$ is the switching ripple voltage of the power converter.

The dc-link component of the output voltage is compensated by the PF capacitor and the series inductors filter out the switching frequency of the power converter. Given that the utility does not represent the dc voltage component, the dc component is regarded as a short circuit and the power converter is represented as two dc voltage sources in phases *a* and *b*. Considering that the series inductor and capacitor are under the steady state, the dc voltage source is regarded as capacitance and the inductor is regarded as a short circuit. Therefore, the suitable rated capacitor having the dc voltage component is represented by expression (9).

$$V_{pha(\mathrm{dc})} = V_{phb(\mathrm{dc})} = \frac{v_{dc}}{2}$$
$$V_{phc(\mathrm{dc})} = -v_{dc} \tag{9}$$

where $V_{phc(dc)}$ is the dc voltage component across the series capacitor in phase *c*.

The fundamental frequency voltage component is examined and regulated with the dc voltage component. At the fundamental frequency, the coupling inductor and series capacitor represent a capacitive characteristic to stop the excessive fundamental current through APF. The impedance of the inductor is small and negligible compared with the capacitor set. The series capacitor provides necessary fundamental reactive power and blocks the redundant fundamental current through APF to withstand the utility fundamental.

C. Reactive power compensation capability

When the passive power component in expression (4) and (7) is a pure inductor value (L_F), the APF acts similar to a traditional pure APF. When the passive power component consists of a series connection of an inductor (L_F) and a capacitor (C_F), the APF behaves similar to an HAPF with leading capacitive (C_F) controlling the passive values at the fundamental frequency. In steady state condition, given the dc-link voltage controller ($I_{cFxfp} = 0$), ($X_{Ff} = X_{LFf}$) for pure APF and ($X_{Ff} = -|X_{cFf} - X_{LFf}|$) for *LC*-HAPF. The ($Q_{Cf}$) present a fundamental reactive power injection with negative signs as the inductive loading compensation [18]. The ratio between the dc-link voltage and the load voltage ($R_{v_{dc}}$) determines the operational range of the APF. The dc voltage value (v_{dc}) of the APF must be larger than the peak of the load voltage, regardless of the coupling inductance (L_F); the inverse setting is required for the HAPF. Therefore, the APF cannot support the inductive loading compensation when it operates as a pure PF [19].

On the contrary, the HAPF can exhibit such support depending on the passive parameters because of the fixed reactive compensation (Q_{Cf}). The fundamental voltage component across the series capacitors causes fixed reactive power compensation, as suggested in expression (10) of study [20].

In the proposed two-leg VSI topology, the fixed reactive power compensation phenomenon is limited in the single

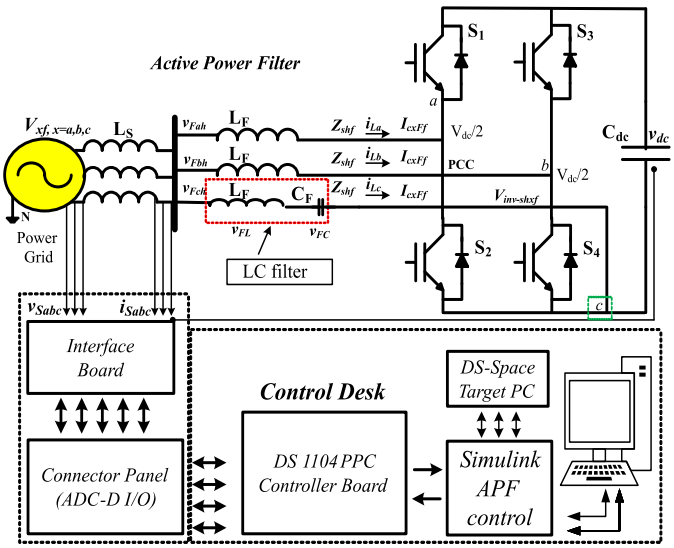

Fig. 3. Circuit schematic of the proposed SAPF system

reduced leg compared with other two phases. The reason is that the tuned LC filter without APF provides higher reactive power capacity than the tuned LC filter with APF.

$$Q_c\,(MVAr) = (2\pi f) \times (cv_s^2) \tag{10}$$

where c is the capacitance of the capacitor, v_s is the mean value of the source voltage, and ω is the fundamental frequency. As notice the maximum reactive power compensation capacity depends on the impedance value (Z_{sh} = inductive) in the three-phase APF as expressed as

$$Q_{shf}\,(MVAr) = 3 \times (\frac{V_{pcc}^2}{Z_{sh}}) \tag{11}$$

To compensate the reactive power, the voltage of the VSI inverter is greater than the PCC voltage as written as ($V_{sh} > V_{pcc}$). As we noticed, that the (θ_{shv}) is very small as compare to the (θ_{shi}), due to the (θ_{shz}). Hence the ac inductors impedance is inductive, so the (θ_{shz}= 90^o), therefore resulting the active fundamental power shift from the APF inverter to the point of common coupling PCC is zero as

$$P_{shf} = \left(\frac{V_{pcc}.\mathrm{V}_{sh}}{Z_{sh}}\cos\theta_{shv} - \frac{V_{pcc}^2}{Z_{sh}}\right)\cos\theta_{shz} \rightarrow \mathrm{P}_{shf} = 0$$

$$Q_{shf} = \left(\frac{V_{pcc}.\mathrm{V}_{sh}}{Z_{sh}}\cos\theta_{shv} - \frac{V_{pcc}^2}{Z_{sh}}\right)\sin\theta_{shz} \rightarrow Q_{shf} = V_{pcc}.I_{sh} \tag{12}$$

$$H_{sh} = \frac{V_{pcc}.\mathrm{V}_{sh}}{Z_{sh}}\sin\theta_{shz} \rightarrow H_{sh} = V_{pcc}.I_{sh}$$

where V_{sh} is the VSI output voltage, V_{pcc} is the voltage at PCC, θ_{shi} is the capacitance of the capacitor, θ_{shz} is the mean value of the source voltage, and θ_{shv} is the fundamental frequency.

The VA rating of the APF inverter for reactive and harmonic power compensation as presented in expression (13) and (14) as follow, where P_{loss}, represents the total active power loss of the APF. The I_{sh}, is the compensating currents, R_{sh} is the switching losses in each phase of the VSI inverter.

$$VSI_{q-rating} = S_{q-vsi} = \sqrt{\left(Q_{shf}^2 + P_{loss}^2\right)} \tag{13}$$

$$VSI_{h-rating} = S_{h-vsi} = \sqrt{\left(H_{shf}^2 + P_{loss}^2\right)} \tag{14}$$

$$P_{loss} = 3\left(I_{sh}^2.R_{sh}\right)$$

In the steady state, the active fundamental current (I_{cFxfp}) shows the minimum value (($I_{cFxfp} \approx 0$). However, the APF inverter injects pure reactive fundamental current equal to $\left(I_{cFxf} = jI_{cFxfq}\right)$. Hence, ($V_{inv-shxf}$) in expression (15) verifies the pure active component as

$$V_{inv-sxfp} = V_{inv} + I_{inv-sxfq}(\mathrm{X}_{cFf} - \mathrm{X}_{LFf}) \tag{15}$$

At full compensation power of the PF, the HAPF compensating reactive power (Q_{Cf}) is equal to the reactive power provided by the passive component (Q_{CFf}), which can be expressed as expression (16). In this equation, $Q_{CFf} < 0$ proofs the injecting reactive power as the leading reactive power.

$$Q_{cFf} = -\frac{V_x^2}{\left|X_{cFf} - X_{LFf}\right|} < 0 \tag{16}$$

D. Filtering characteristic of the proposed APF model

A three-phase equivalent circuit of the proposed configuration is illustrated in Fig. 4 (a). The APF is used as a regulated voltage source (V_{AF}) with two independent control source (V_S) and (I_L) and a filter impedance ($\mathrm{Z_F} = Z_{Fabc}$) to compensate for the specific harmonics of interest. In practical system, operating the load as a model harmonic current source is difficult because of the system impedance [21]. However, in the equivalent circuit, the non-linear load is considered a model current source (I_L) with pure sinusoidal waveforms. The APF operates as the voltage source proportional to the component of line current harmonics ($\mathrm{V_{AF}} = K \times I_{sh}$), where K represents the gain of the filter, I_{sh} shows the source current, I_{Fh} is the APF compensation current and I_{Lh} is the load current.

At low harmonic frequency, the VSI operates as an inductor and advances to stop the flow of fundamental current in the APF branch. However, keeping the high K value reduces the resonance and background harmonic voltage [21, 22]. For reactive current damping, the passive filter operates without controlling the voltage source as shown in Fig. 4 (b), and the

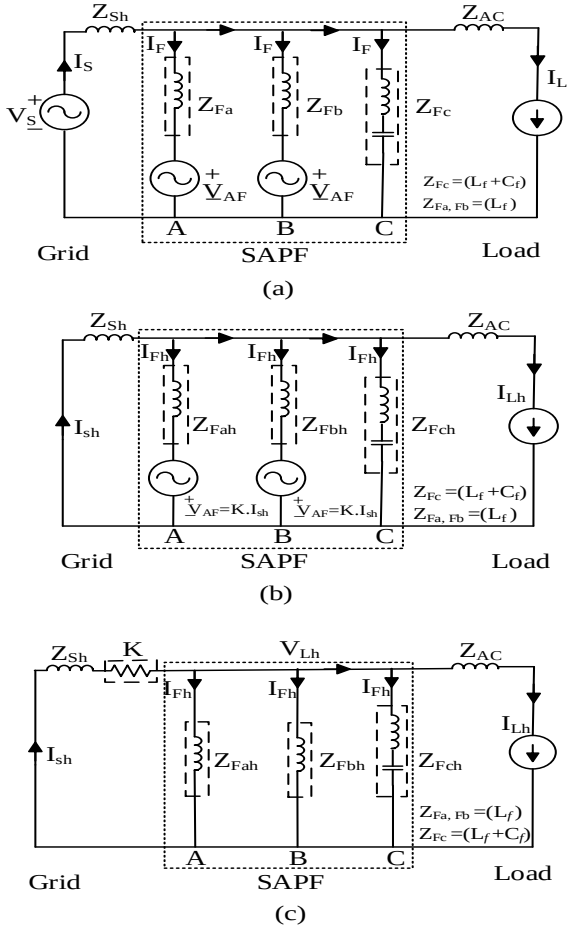

Fig. 4. (a) Total equivalent circuit of a three-phase system (b) three-phase harmonic equivalent component circuit (c) Resistive equivalence of harmonic filter.

utility is studied as a pure sinusoidal source. Applying Kirchhoff's voltage law (KVL), we calculated the following expression (17).

$$V_{sh} - I_{sh}Z_{sh} - I_{Fh}Z_{Fh} - V_{af} = 0 \quad (17)$$

$$\text{Where, } V_{sh} = 0, \text{ and } V_{af} = KI_{sh} \quad (18a)$$

$$I_{sh} = I_{Lh} + I_{Fh} \quad (18b)$$

Combing the equations (18a) and (18b), the ratio $\frac{I_{sh}}{I_{Lh}}$ between the harmonic line current and the non-linear load, when no APF is connected (K = 0) is presented in expression (19).

$$I_{sh} = \left(\frac{Z_{Fh}}{Z_{Fh} + Z_{sh}}\right) \times I_{Lh} \quad (19)$$

The excellent filtering characteristic depends on the impedance value ($Z_{Fh} \lll Z_{sh}$), where Z_{Fh} is the PF impedance ($Z_F = Z_{Fabc}$) and Z_{sh} is the system impedance. Fig. 4 (c) shows that the APF operates similar to a practical impedance [23] in series with the source impedance (Z_S) to operate as a pure resistor (K = Ω).

At the fundamental frequency, the APF operates at zero impedance but follows the inductor path at harmonic frequencies in expression (19). During the APF operation, the K value determines the flow of the harmonic and stops the harmonic by pushing toward the APF leg [24]. However, the APF follows the inductor path at harmonic frequencies, as shown in expression (20).

$$\frac{I_{sh}}{I_{Lh}} = \frac{Z_{Fh}}{K + Z_{Fh} + Z_{sh}} \quad (20)$$

The K value is always kept higher than the impedance Z_S value to improve the filtering characteristic and prevent the stability and resonance problems between Z_S and Z_F.

1) *APF capability to improve filtering performances:* The feedback control gain K suppresses the resonance between the utility grid and the PF is shown in Fig. 3 and Fig. 4 (c). The LC filter is tuned to 250 Hz and 400 Hz frequency to suppress the harmonics below and above the tuning frequency. Therefore, the tuning frequency is range in between the 200 and 550 Hz. It is worth to note that the rectifier load produces fewer harmonic at 11th and 13th harmonic frequencies, so these harmonics are not a series issue. Therefore, the LC-filters in tuned at 5th and 7th dominant harmonics in between the grid phase and DC-link capacitors as shown in Fig. 5 (a) and (b). These results verify the filtering capability of proposed APF is satisfactory at 5th (250 Hz) and 7th (352 Hz) harmonic frequencies.

Fig. 6 shows a bode plot of the filtering characteristics of the proposed APF. Different K values against the harmonics $I_{sh}/I_{Lh} = \left(\frac{Z_{Fh}}{K+Z_{Fh}+Z_{sh}}\right)$, in expression (20) db and inter harmonic frequencies in Hz, proof the frequency response of the LC filter. When only PF is connected (K=0) in expression (19), the harmonic amplifying phenomena occur at the frequency range between 340 and 350 Hz [17]. However, when the APF is connected (K>0), harmonic damping

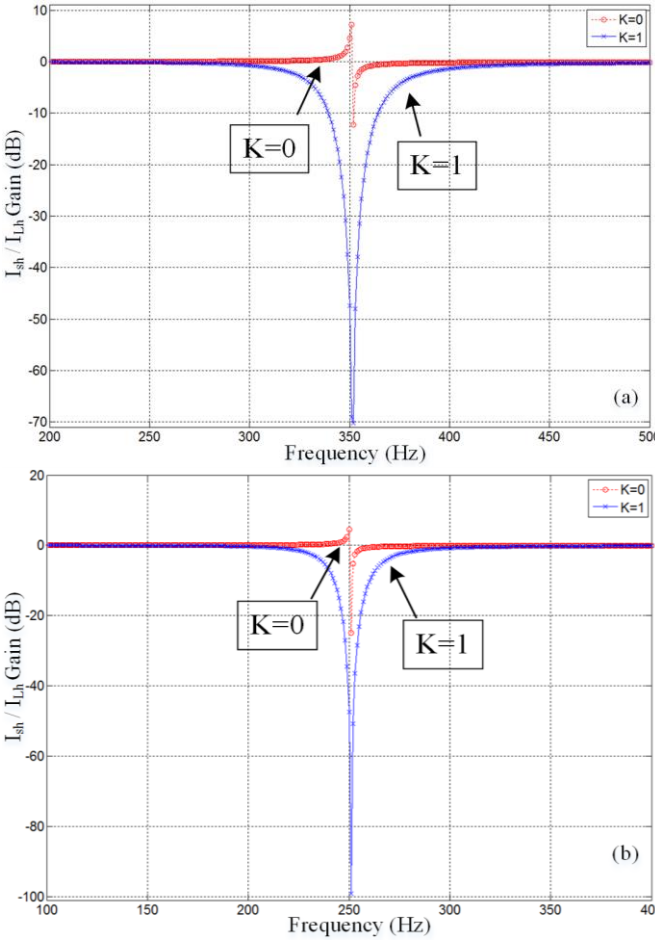

Fig. 5. Capability to improve the filtering performances of APF (K = 0, K = 1) due to tuning frequency: a) I_{sh}/I_{Lh} at 352 Hz. and b) I_{sh}/I_{Lh} at 250 Hz.

increases and no amplification phenomena occurs. In addition, all the harmonic contents components are considerably reduced as shown in Fig. 6. The feedback gain K value range up to infinite values to disappear the harmonic content entirely but its range is limited to certain values due to the stability issues. The problem of harmonic resonance in the PF put the limitation of wider range frequency tuning [17]. Therefore, as notice the use of PF is limited to the single phase of the power converter as compare to other APF topologies. It proof that the proposed APF is capable to improve the filtering performances, no harmonic amplification phenomena and compensate the current harmonic contents produces from the nonlinear rectifier load.

2) *APF capability to enhance system robustness:* In order to proof the system robustness, bode plot of I_{sh}/I_{Lh} in expression (20) is plotted against the different L_S values, when the APF is connected. In (Fig. 7), the harmonic current amplification increases and shift to lower frequency with the increase L_S value and vice versa. Furthermore, the results verifies that the adopted APF does not change the harmonic current compensation characteristic as shown in Fig. 7. Here, both results in Figs. 6 and 7, verifies the proposed APF has capability to enhance the system robustness and to improve the filtering performances.

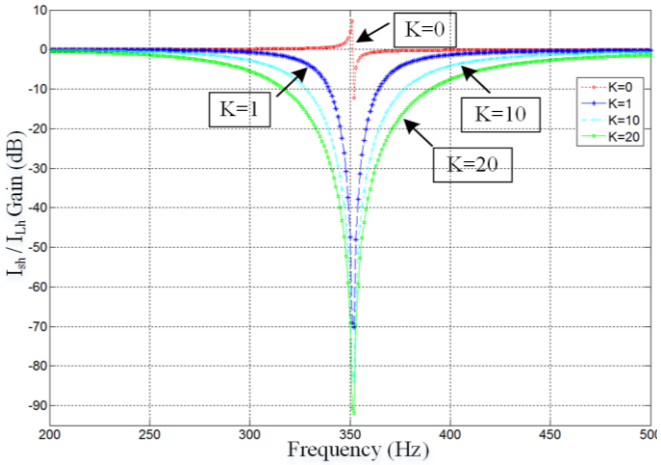

Fig. 6. Filtering characteristics and frequency response of the APF.

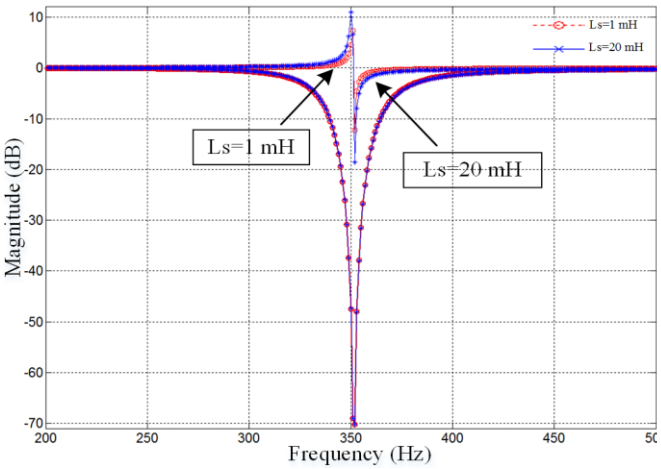

Fig. 7. Capability to enhance the system robustness due to varying Ls: a) without APF (K = 0) and b) APF is employed (K =10).

III. OVERALL CONTROL SYSTEM

A. *Controller reference generator*

The controller is designed to eliminate the current harmonics and maintain constant dc-link voltage. The overall controller operates in three parts: phase lock loop (PLL), APF system reference generator, and dc-link voltage control. The prototype control algorithm is tested in a *dSPACE* modular unit based on a *DS1104* processor board (Fig. 8). The PLL scheme offers transient free locking to the rotating synchronous frame with the positive sequence of the three-phase supply voltages; this scheme is thus used to control the system reference voltage for VSI operation.

An SPWM switching scheme is adopted to compensate the harmonic contents and lower the ripples in the output voltage waveform and consequently avoid the zero utility current. With regard to a proper PWM switching scheme, the modulation signal is compared with the high-frequency triangular wave (V_{tri}). At the fundamental frequency, the three-phase supply current is converted into a two-phase instantaneous active (i_d) and instantaneous reactive (i_q) currents. The zero sequence is neglected because of the three-phase system; thus, the VSI provides the ac voltage to compensate the system harmonics. The active and reactive

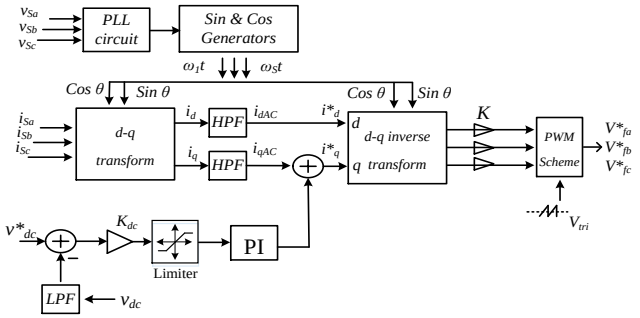

Fig. 8. Overall control system of the proposed SAPF.

quantities are decomposed into dc and ac values at the fundamental frequency (ω1 = 50 Hz). However, the fundamental component is a dc value, and the harmonic components are ac values.

To extract the ac current harmonics into ($i_{d_{AC}}$) and ($i_{q_{AC}}$), two second-order high-pass filters (HPFs) are designed at the cutoff (50 Hz) frequency [21]. The HPF sample time delay affects the performance of the APF and the dynamic voltage damping [8]. In the end of the process, the inverse d-q transformation regenerates the supply harmonic current components. The APF parameters and characteristics are dependent on the K value. The voltage reference (v^*_{AF}) of each phase (v_{Af}, v_{Bf}, v_{Cf}) is amplified by the gain (K) for proper switching gate signals of the PWM inverter.

$$V^*_{AF} = K \times i_{F_{abc}} \tag{21}$$

B. *DC-Link voltage control*

The excessive absorption of the active power increases the dc-link voltage [8], as the leading current in the dc-link capacitor, thereby eliminating the need of external power source. To protect the active filter from being damaged, the value of the reactive dc current ($i_{q_{DC}}$) is injected into the quadrature axis. A proportional integral (PI) controller is thus adopted at the required voltage level of the PWM inverter to compare the reference signal with the detected dc-link voltage for final voltage reference. The PI controller maintains the harmonic current time derivatives for the active filtering operation. However, the voltage reference is maintained higher than the peak value of the ac supply voltage. Therefore, the proportional (K_p) and integral (K_I) gain values are considered as 0.2 Ω^{-1} and 31 Ω^{-1}.

IV. SIMULATION RESULTS AND DISCUSSION

A. *Prototype description*

Figs. 9 (a) and 9 (b) shows the picture of the laboratory prototype of the manufactured APF to validate the performance. To test the performance of the proposed scheme, the voltage source inverter (VSI) consists of two-leg IGBT module (IKW75N60T) which is a (600 V, 85 A) four single module from Infineon, its gate driver SKHI 61R manufactured by SEMIKRON, operating at 20 kHz switching frequency.

The two-leg of the VSI inverter is installed in series with a coupling inductors L_F, while the reduced switch-leg is

This article has been accepted for publication in a future issue of this journal, but has not been fully edited. Content may change prior to final publication. Citation information: DOI 10.1109/TPEL.2017.2728602, IEEE Transactions on Power Electronics

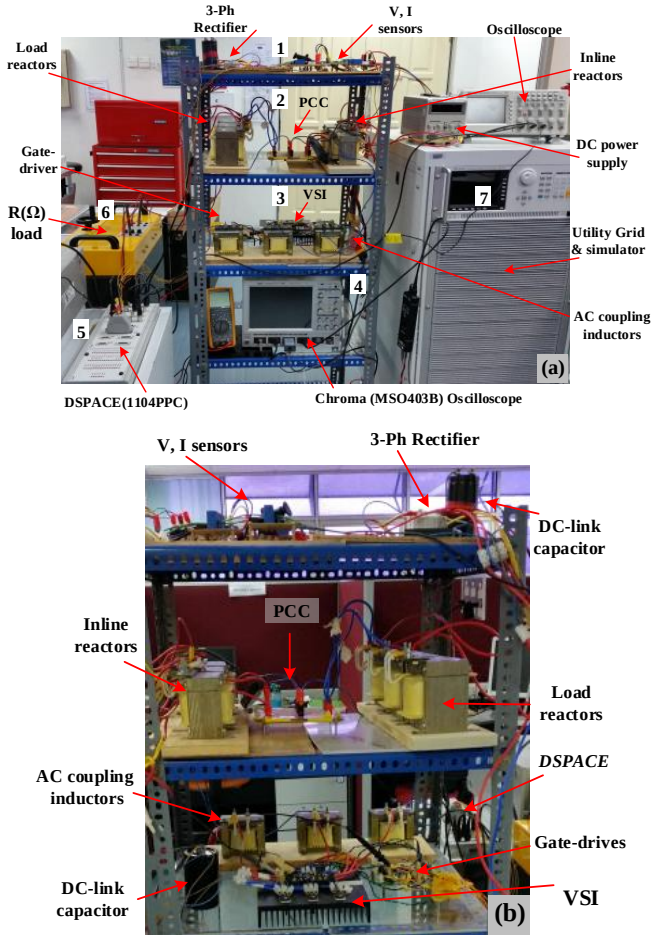

Fig. 9. (a) Hardware setup of a Four-switch two-leg SAPF system test-rig. (b) Zoom snapshot of VSI, DC-bus capacitor and other components.

installed through a passive filter (2.0 kVAR). Two sets of PFs (1.9 mH and 1 mH, 45 A three-phase inductor, and two 200μF 400 V capacitors) are tuned at 5th and 7th harmonics frequencies to mitigate the current harmonics and compensate the reactive power compensation.

The model 61511 from Chroma ATE. INC instruments has been used as a power supply. Hereinafter, the prototype is tested at 200V ac source connected directly with the grid for flexible testing. The design load is a three-phase diode rectifier at dc-side with smoothing capacitor $C_d = 1500\ \mu F$ and resistor of R=40 Ω. The APF system operates at the maximum rating of 2.2 kVA, consisting of 5 kW diode rectifier load, with the (4700 μF, 300 V) dc-link capacitor. Therefore, the dc-link capacitor rating is designed to operate at voltage ripple less than 10%. To compensate the 5kW diode rectifier load system, a 2.2kVA APF system and 2.0kVAR PFs system is satisfactory to mitigate the harmonics and reactive power compensation. The complete experimental and simulation system parameters are listed in Table I, Table II, and Table III.

B. *Performance evaluation under steady-state load condition*

To understand the performance of the proposed system, a simulation model with same parameters mention in Table I, has been extensively simulated in Matlab-Simulink

TABLE I
EXPERIMENTAL SYSTEM SPECIFICATIONS.

Parameters	Value	Unit	Symbol
Diode Rectifier rating	5	kW	-
Line to line RMS voltage	200	V	(v_s)
Output RMS voltage	200	V	V_{out}
Grid Frequency	50	Hz	-
Supply Inductor	0.21	mH	(L_s)
AC load inductor	3	mH	(L_{AC})
Rectifier DC capacitor	1500	μF	(C_d)
Nonlinear load resistor	40	Ω	(R)

TABLE II
PARAMETERS OF THE APF.

Parameters	Value	Unit	Symbol
Active filter rating	2.2	kVA	
Filter AC Inductor	1.9	mH	(L_F)
DC capacitor of APF	4700	μF	(c_{dc})
DC voltage of APF	300	V	(v_{dc})
HPF Cut off frequency	50	Hz	(F_{HPF})
Gain	11	Ω (p.u)	(K)
Switching Frequency	20,000	Hz	f_{sw}
Switches Types	Infineon IKW75N60T		$S_1 - S_4$

TABLE III
PARAMETERS OF THE PF.

Parameters	Value	Unit	Symbol
Passive filter rating	2.0	kVAR	
Filter inductor	1.9	mH	(L_F) (5th)
Filter Capacitor	200	μF	(C_F) (5th)
Filter inductor	1	mH	(L_F) (7th)
Filter Capacitor	200	μF	(C_F) (7th)
Resonance frequency (PF)	258	Hz	(5th)
Resonance frequency (PF)	357	Hz	(7th)
Quality Factor	57	-	(Q)

environment. Frequently, the simulation waveforms are recorded in the following sequence: utility voltage v_{Sabc}, utility current i_{Sabc}, load current i_{Labc} filter compensation current i_{Fabc} and dc-link capacitor voltage v_{dc}. Fig. 10 shows the simulation results of the utility voltage, source current, load current, and filter compensating current. As notice both the load current and source current is seriously distorted because of the three-phase rectifier load with THDi of 30.1%. As observed after compensation, the source current is sinusoidal waveform and the load current is distorted waveform.

The dc-link voltage of the APF is maintained constant without the need of external dc power supply as shown in Fig. 11. As notice at the point of injection, the dc-link voltage rise nearly up to 10% and remain constant during the step change presenting no stability problem. Therefore, the dc-link voltage is kept constant at 300V to control the voltage references for feedback control and enhanced reactive power demand. The dc voltage ripple offset at the fundamental frequency is stopped, due to the capacitive effect in phase (a, b) but in phase (c), the LC passive capacitor prevents the dc current flow towards the power supply, with the minimum value of ripple without amplification phenomenon at dominant harmonic frequency.

This article has been accepted for publication in a future issue of this journal, but has not been fully edited. Content may change prior to final publication. Citation information: DOI 10.1109/TPEL.2017.2728602, IEEE Transactions on Power Electronics

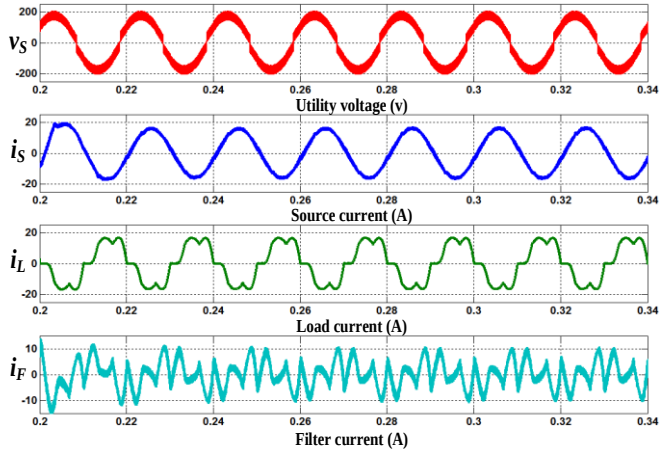

Fig. 10. Steady state operation of the proposed SAPF a) Utility voltage (THD*v*=4%) b) Utility current (THD*i*=4.1%) c) Load current (THD*i*=30.1%) d) Compensating filter current.

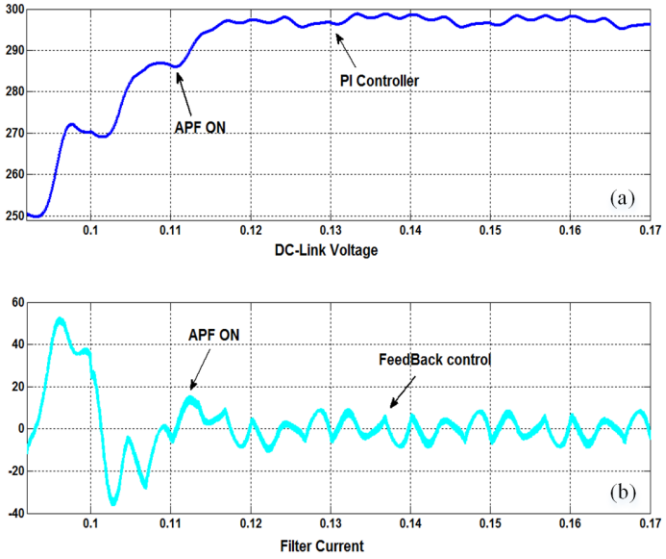

Fig. 11. a) DC voltage (50V/div). b) Filter current (100A/div) at filter switched ON (t=0.15).

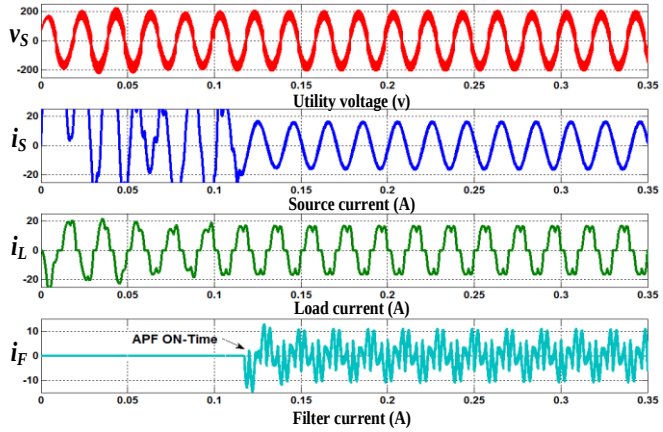

Fig. 12. Starting performance of the proposed SAPF. a) Utility voltage (THDv=4%) b) Utility current (THDi=4.1%) c) Load current (THDi=30.1%) d) Compensating current at switched ON.

To check the proposed APF accuracy and stability, after a time of t=0.12 ms the APF is tested the switching filter start time operation, it inject the filter compensating current into the transmission line. The starting performance of the proposed

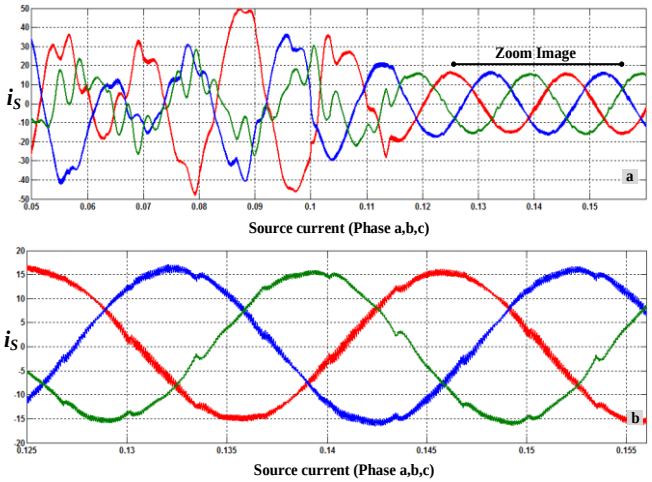

Fig. 13. a) On-state and Off-state APF operations. b) Zoom image of utility line current (i_{Sabc}) at 5th and 7th order harmonics.

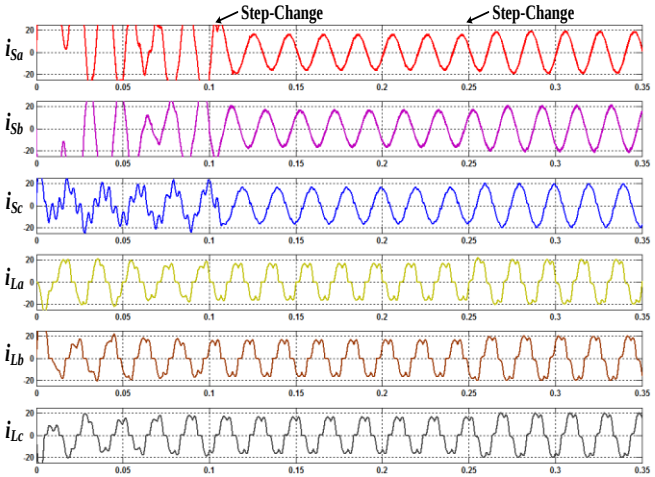

Fig. 14. Dynamic performance with the R-L load step-change waveforms of the proposed SAPF.

APF to compensate the reactive power and harmonics current mitigation is depicted in Fig. 12. The load current and utility current waveforms are seriously distorted but as soon as the active filter is inserted, the utility current is a stable and sinusoidal waveform. The THD of the supply current is dropped from 30.1% (without APF) to 4.1% (with APF) effectively. Furthermore, the harmonic contents of source and load current per phase of three-phase SAPF system are summarizes in Table IV (5th PF tuned). The two-leg APF model is coupled with LC PF tuned at 5th order dominant harmonic frequency. Here, after applying the APF and PF filter, THD*i* of the supply current is satisfactory in the phase *a* and phase *b* (<5.0%) respectively, however unsatisfactory performance followed in phase *c* (>5.0%).

The harmonic compensation of PFs performance is evaluated into two states of operation: On-state and Off-state. The single tuned PF filtering performance is not good at the current harmonics are given in Table IV (5th PF tuned). As depicted in Figs. 13 (a), and (b), together both the sets of PFs drop the THD_i from 31.36% (without PF) to 3.61% (with PF) against the dominant order 5th and 7th harmonics frequencies, as shown in the Table IV (5th and 7th PF tuned).

This article has been accepted for publication in a future issue of this journal, but has not been fully edited. Content may change prior to final publication. Citation information: DOI 10.1109/TPEL.2017.2728602, IEEE Transactions on Power Electronics

TABLE IV
SOURCE CURRENT HARMONIC CONTENTS.

Order Harmonics	Peak Current Before Compensation			Peak Current After Compensation (5th PF tuned)			Peak Current After Compensation (5th and 7th PF tuned)		
	i_{sa}(A)	i_{sb}(A)	i_{sc}(A)	i_{sa}(A)	i_{sb}(A)	i_{sc}(A)	i_{sa}(A)	i_{sb}(A)	i_{sc}(A)
Fundamental	100	100	100	100	100	100	100	100	100
3rd	0.2	0.24	0.01	0.2	0.07	0.14	0.05	0.09	0.1
5th	19.51	19.57	19.76	0.9	0.87	0.98	0.79	0.97	0.69
7th	7.29	7.48	7.16	2.13	2.55	4.66	0.36	0.41	0.29
9th	0.03	0.04	0.06	0.08	0.18	0.12	0.08	0.12	0.07
11th	2.64	2.60	2.55	1.45	0.85	2.28	0.96	0.54	1.41
13th	2.13	2.16	2.06	0.68	1.3	1.98	0.54	0.98	1.48
15th	0.05	0.02	0.06	0.1	0.04	0.06	0.05	0.1	0.06
17th	1.32	1.30	1.30	0.77	0.5	1.27	0.72	0.39	1.1
19th	0.98	1.01	0.94	0.33	0.61	0.94	0.31	0.52	0.82
21st	0.02	0.01	0.01	0.18	0.3	0.51	0.01	0.05	0.06
THD	31.20	31.32	31.36	4.86	4.73	6.04	4.06	3.93	3.61

C. Performance evaluation under transient-state load condition

In order to verify the transient filtering performance of the proposed model, the standard tests has been carried out. Fig. 14, shows the dynamic performance of the proposed APF during the step-on load change for R-L and inductive (VAR) non-linear loads. The step change starts at time t=0.1 ms and other at time t=0.25 ms to response the settling time for compensating the step load change effect in less than one cycle. It is noticed that the proposed APF compensate the unbalance impedance ratio effect in each phase and operate as conventional APF. It provides the necessary negative sequence compensation at the step-change with less unbalanced source current waveform for the only R-L load.

V. EXPERIMENTAL RESULTS AND DISCUSSION

A. Performance evaluation under steady-state load condition

The measured experimental results including the utility line current THD, line voltage THD, cost and size analysis, all these results validate the simulation waveforms. The developed results validates the configured power stage of the full-bridge inverter implemented using the two-leg VSI stage. All the experimental data are recorded by Lecroy Wave Runner 500 MHz digital scope.

The experimental results shown in Fig. 15, verify the active filtering of the proposed APF; specifically, the grid source current THD_i is reduced from 30.1% to 4.1%. Though, connected with the three-phase rectifier load; the load current is distorted but after compensation the utility current have been changed to sinusoidal waveform and harmonic load current meet the IEEE 519 standards. Here, the waveforms are recorded in the following order such as; utility voltage v_{Sa}, load current i_{La}, and source current i_{Sa} respectively. The simulation and experimental comparison results verify the effectiveness of the proposed APF for mitigating the load current harmonic to meet the IEEE 519 standards. It can be seen from these results that the THD of the utility current and utility voltage are below (5%) even for severe operating condition. However, the control gain is set to a high value (K = 11Ω) for excellent filtering characteristics. The fundamental voltage to the inverter exhibits large amount of switching ripple because of the PWM. Hence, the series inductor with the power converter eliminates these switching ripples. The output filter compensating current (i_F) for APF have been

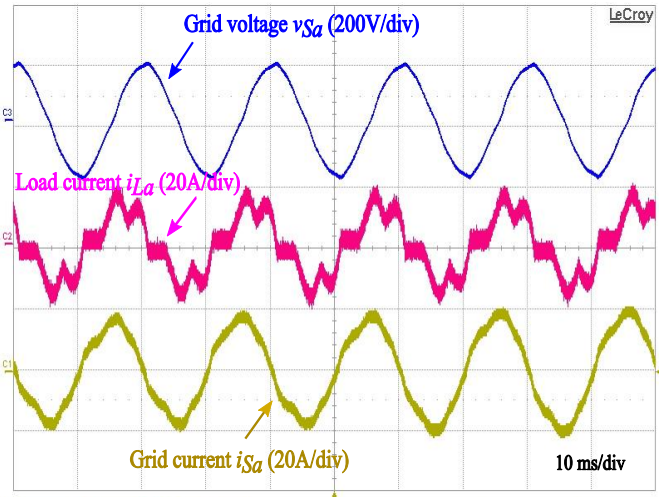

Fig. 15. Experimental result for the active power filtering mode a) Utility voltage (THDv=4%) b) Load current (THDi=30.1%) c) Utility current (THDi=4.1%).

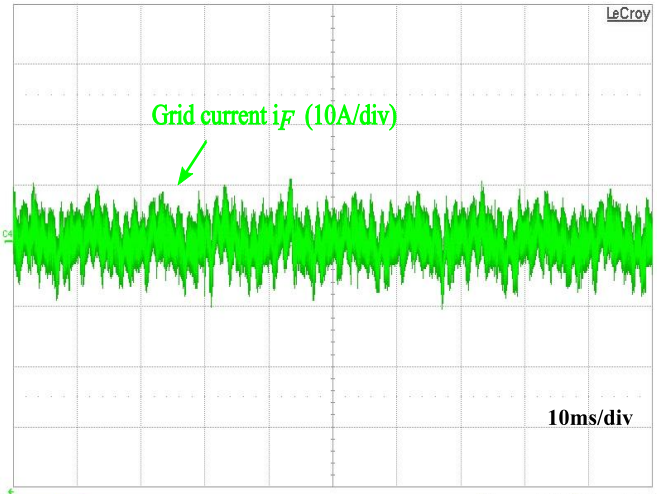

Fig. 16. Experimental result of the proposed SAPF, Filter compensating current waveforms.

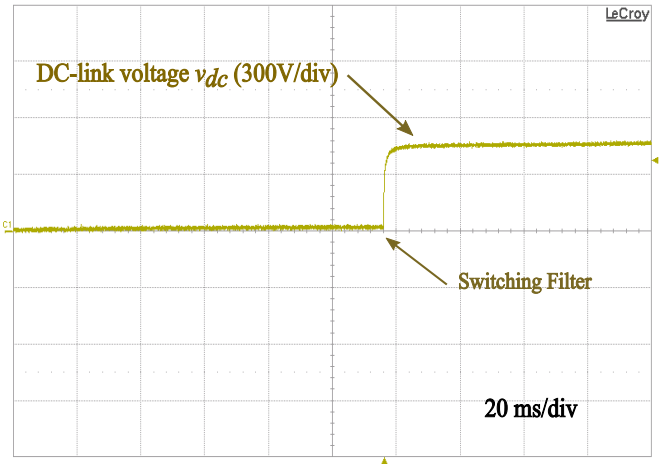

Fig. 17. Testing of dc-link voltage controller at filter switched ON.

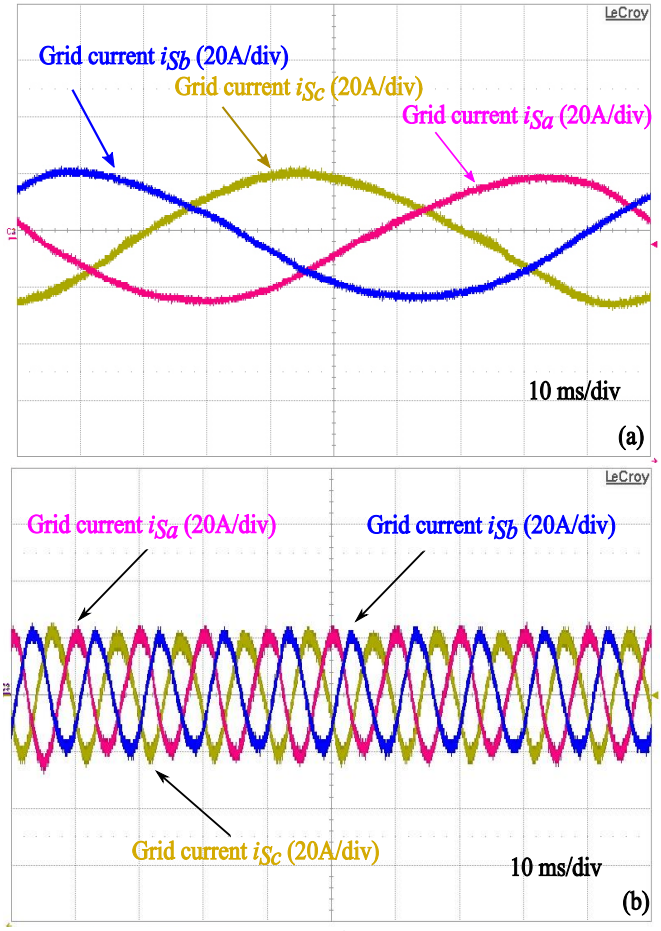

Fig. 19. Steady state operation of the proposed SAPF. a) Utility current (i_{Sabc}). b) Zoom image of utility current (i_{Sabc}).

shown in Fig. 16. The waveforms comprises a high order harmonics generated due to switching operation of the two-leg VSI.

To test the dc-link voltage controller and its stability, the experimental results for dc-link voltage before and after load step-change is demonstrated in Fig. 17. An appropriate control produces a stable and constant dc-bus voltage. The experimental results are very close to simulation proof effective reactive power compensation features of the APF system. Therefore, Fig. 17 show the switching filter start point after time t=0.12 ms as the APF start the operation.

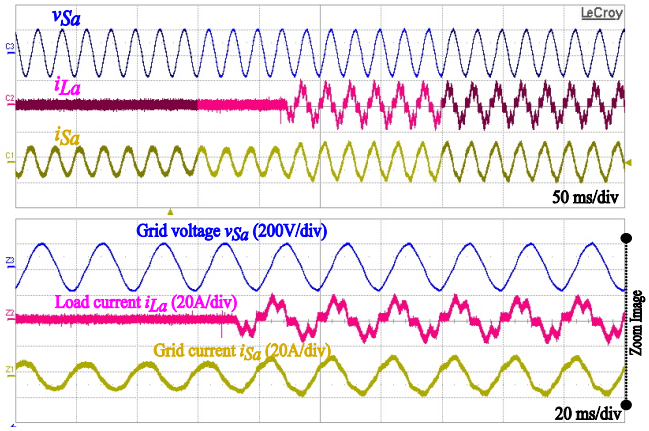

Fig. 20. Experimental results under transient condition at (0% to 100%) step load. a) Utility voltage b) load current c) utility current.

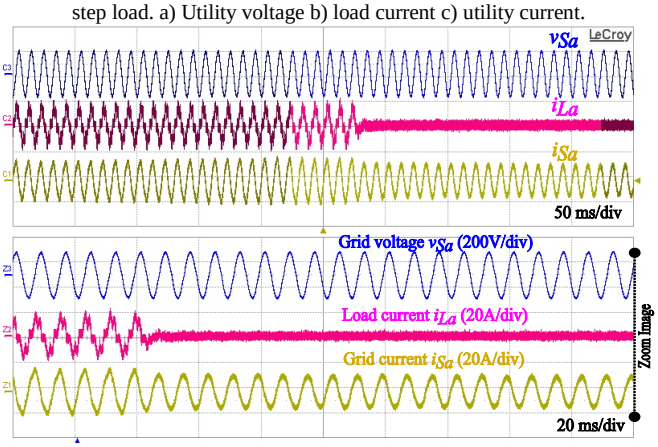

Fig. 21. Experimental results under transient condition at (100% to 0%) step load. a) Utility voltage b) load current c) utility current.

The proposed APF is a low-cost structure and successfully reduces power devices for providing harmonic and reactive power compensation. In verifying this deduction, the utility current in each of the three phases is shown in Fig. 18. In figure, the proposed APF system injects different compensating currents to control the load current demand in each phase. Also, it operates as expected even with reduced switch devices against the critical problems in the power distribution system.

Fig. 18 illustrate the comparison of the compensating and un-compensating source current before and after filtering with two sets of PF. However, a large amount of 5th and 7th harmonic exits in the uncompensated source current before the APF filtering. The system offers the best response after filtering at fixed load and step load change.

The LC filter tuned at 5th and 7th harmonic frequencies reduces the flow of non-negligible amount of harmonics in the system, with THD*i* values from 30.1% (without APF) to 3.61% (with APF). The comparison of the source THD values, show a significant improvement in the THD with the dual sets of LC PF and two leg APF for non-linear loads. Here, after compensation, the THD*i* of the source current is successfully reduced, which validates that the proposed APF system, effectively compensates the current and voltage THD.

Roughly, the same experimental result is obtained using the same equivalent system parameters and control scheme. After compensation, the three-phase utility currents are nearly

This article has been accepted for publication in a future issue of this journal, but has not been fully edited. Content may change prior to final publication. Citation information: DOI 10.1109/TPEL.2017.2728602, IEEE Transactions on Power Electronics

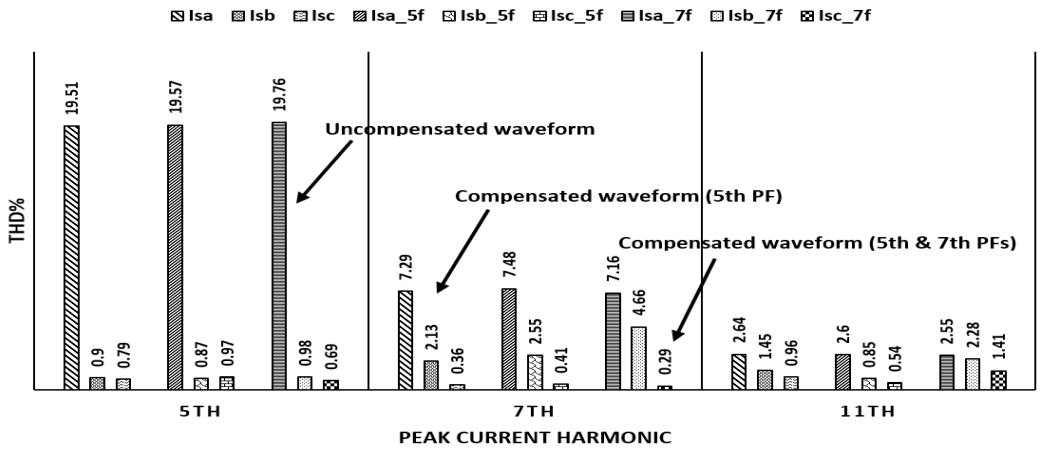

Fig. 18.Spectral analysis of the source current (5th PF tuned).

TABLE V
COMPARISON FOR INVERTER COST, WEIGHT, VOLUME AND OTHERS PARAMETER.

	Values			Reduction		Actual Value	
Reference	No. of switches	Volume (cm^3)	Weight (g)	Volume (cm^3)	Weight (g)	Cost ($)	THD (%)
[21]	6	10.638	36.02	-3.546	-18	39.06	<5
[10]	4	7.092	24.01	0	-18	26.04	<5
[9]	6	10.639	36.02	-3.546	-6	39.06	<5
[25]	9	15.957	54.03	-5.319	-30.01	58.59	<5
Proposed	4	7.092	24.01	-	-	26.04	<5
Type	Single Module IKW75N60T, IGBT Transistor, 600V/80A, Dimensions (21.10 x 16.13 x 5.21mm), weight (6.0042 g), volume = 1773.18703mm, 1.773(cm^3), Cost (6.51)$/each						

TABLE VI
COMPARISON FOR WEIGHT, VOLUME AND COST FOR CAPACITOR.

	Values			Reduction		Actual Value
Reference	No. of Capacitor	Volume (cm^3)	Weight (g)	Volume (cm^3)	Weight (g)	Cost ($)
[21]	3	27.051	180	-18.034	-120	282.24
[10]	3	27.051	180	-18.034	-120	282.24
Proposed	2	18.034	120	9.017	60	188.16
Type	Film Capacitor, PP (Polypropylene), 330VAC/50A, 200 µF, Dimensions (63.5 x 142mm), diameter (142mm), weight (60 g), volume = 9017mm, 9.017(cm^3), Cost (94.08)$/each					

sinusoidal with reduced switch count devices, as noticed in Figs. 19 (a) and 19 (b), respectively. The three-phase utility current validates that the proposed two-leg APF effectively compensates against the predominant current harmonics.

B. Performance evaluation under transient-state load condition

Fig. 20 and Fig. 21 illustrate the results under the step-on and step-off load conditions. During the step change operation, the load is sharply decreased from 0% to 100%, and vice versa. The response and recovery time are fast between the changeovers, thereby demonstrating the excellent compensation capability of the proposed APF scheme. The source current remains sinusoidal without aggregating the THD. The source current THD of the APF system decreases by 4.1%, which is within the IEEE-519 standard of 5.0%. With increasing and decreasing load, the proposed APF compensates the voltage drop caused by the energy storage requirement across the dc-link capacitor. The dc controller compensates the voltage effect by increasing and decreasing the supply current asset according to the reference value. The simulation and experimental results verify that the proposed APF scheme provides reactive and harmonic load current compensations under dynamic and steady states.

C. Performance comparison of the proposed APF system

Tables V and VI compares the new designed inverter and capacitors with other existing topologies in terms of cost, weight, volume, number of switches, efficiency, and THD. The novel circuit presents the best reduced weight and volume compact structure compared with other topologies. The overall reduction in weight, volume, and cost is due to the decreased amount of VSI switches and series coupling ac capacitors as illustrated in Fig. 22 (a) [9, 10, 21, 25], and Fig. 22 (b) [10, 21].

VI. CONCLUSION

In this paper, a novel three-phase reduced switch count and transformer-less APF circuit, operating with the function of active filtering and enhanced reactive power compensation. The main point of the proposed APF circuit topology, which uses a two-leg bridge structure and only four IGBT power devices in the three-phase power converter. Compared with the other existing topologies, the elimination of the transformer and minimum active and passive component contributes to a significant reduction in the manufacturing cost, volumetric size and weight.

The proposed APF system is more robust, efficient and

This article has been accepted for publication in a future issue of this journal, but has not been fully edited. Content may change prior to final publication. Citation information: DOI 10.1109/TPEL.2017.2728602, IEEE Transactions on Power Electronics

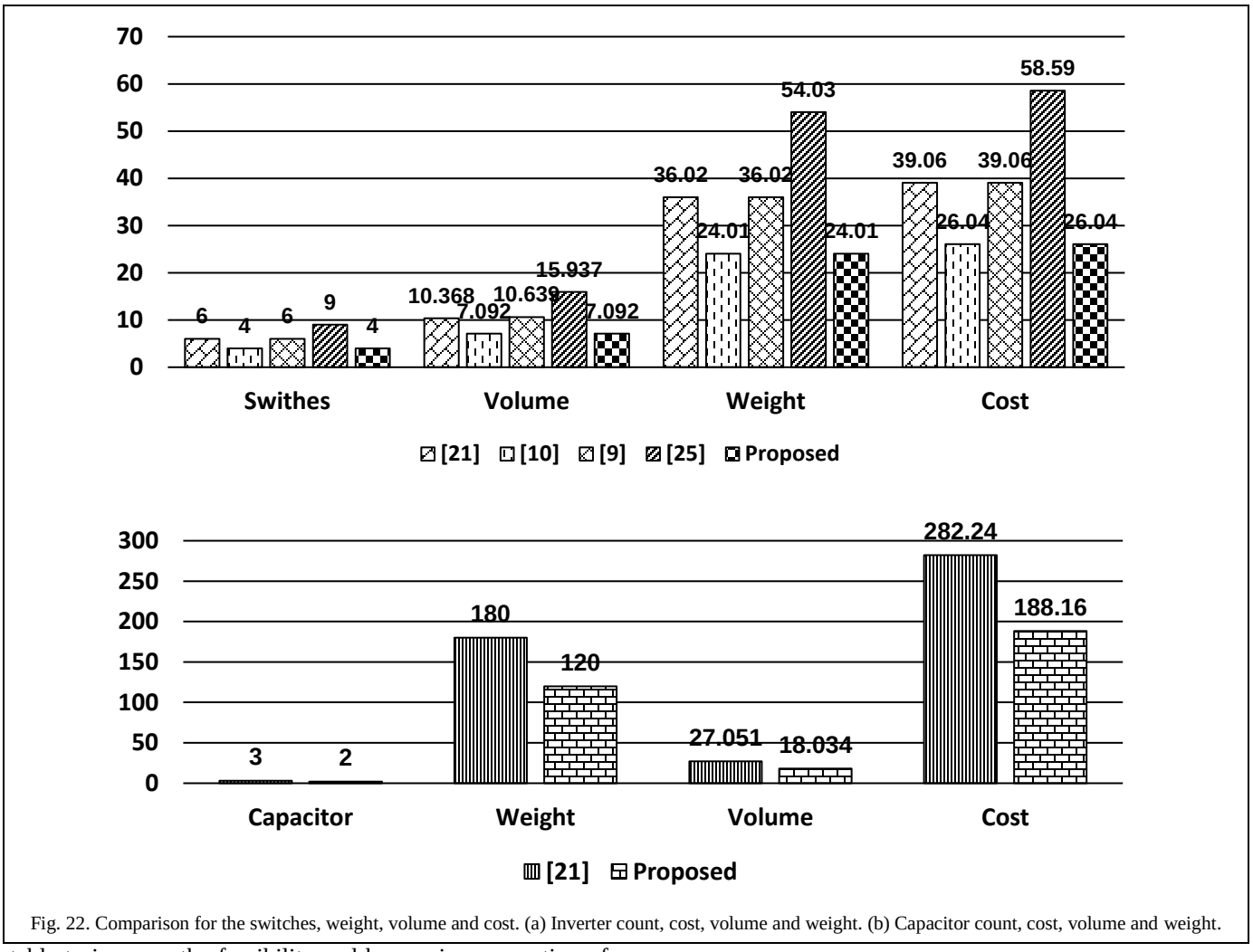

Fig. 22. Comparison for the switches, weight, volume and cost. (a) Inverter count, cost, volume and weight. (b) Capacitor count, cost, volume and weight.

stable to improve the feasibility and harmonic propagation of the power distribution system. A detail analysis of the both the active filter inverter and passive filter, including the reactive power capability and filtering characteristics has been presented. The series LC tuned PF at the 5th and 7th order harmonic frequencies improves the harmonic mitigation performance. However, the series ac coupling inductors can overcome the fixed reactive power compensation caused by the defined value of the LC filter. The control algorithm can ensure the regulated sinusoidal voltage, phase amplitude, and low THD in the power distribution system, along with dc-link voltage control. The experimental and simulation results have verified the feasibility of the proposed APF topology and its excellent performance in terms of both transient and steady states responses to compensate selectively either the reactive power compensation, as well as in damping out the current harmonic distortion. Furthermore, the proposed APF system based on transformerless and power switching device reduced count configuration could be used in extensive applications, such as the grid-connected power converters, grid interfaced distributed energy sources, and so on.

REFERENCES

[1] S. D. Swain, P. K. Ray, and K. B. Mohanty, "Improvement of Power Quality Using a Robust Hybrid Series Active Power Filter," *IEEE Transactions on Power Electronics*, vol. 32, pp. 3490-3498, 2017.

[2] A. Javadi, A. Hamadi, L. Woodward, and K. Al-Haddad, "Experimental Investigation on a Hybrid Series Active Power Compensator to Improve Power Quality of Typical Households," *IEEE Transactions on Industrial Electronics*, vol. 63, pp. 4849-4859, 2016.

[3] W. U. Tareen, S. Mekhilef, M. Seyedmahmoudian, and B. Horan, "Active power filter (APF) for mitigation of power quality issues in grid integration of wind and photovoltaic energy conversion system," *Renewable and Sustainable Energy Reviews*, vol. 70, pp. 635-655, 4// 2017.

[4] J. Solanki, N. Fröhleke, and J. Böcker, "Implementation of Hybrid Filter for 12-Pulse Thyristor Rectifier Supplying High-Current Variable-Voltage DC Load," *IEEE Transactions on Industrial Electronics*, vol. 62, pp. 4691-4701, 2015.

[5] L. Asiminoaei, C. Lascu, F. Blaabjerg, and I. Boldea, "Performance Improvement of Shunt Active Power Filter With Dual Parallel Topology," *IEEE Transactions on Power Electronics*, vol. 22, pp. 247-259, 2007.

[6] T. L. Lee and S. H. Hu, "An Active Filter With Resonant Current Control to Suppress Harmonic Resonance in a Distribution Power

System," *IEEE Journal of Emerging and Selected Topics in Power Electronics*, vol. 4, pp. 198-209, 2016.

[7] S. Rahmani, A. Hamadi, K. Al-Haddad, and L. A. Dessaint, "A Combination of Shunt Hybrid Power Filter and Thyristor-Controlled Reactor for Power Quality," *IEEE Transactions on Industrial Electronics*, vol. 61, pp. 2152-2164, 2014.

[8] R. Inzunza and H. Akagi, "A 6.6-kV transformerless shunt hybrid active filter for installation on a power distribution system," *IEEE Transactions on Power Electronics*, vol. 20, pp. 893-900, 2005.

[9] L. R. Limongi, L. R. d. S. Filho, L. G. B. Genu, F. Bradaschia, and M. C. Cavalcanti, "Transformerless Hybrid Power Filter Based on a Six-Switch Two-Leg Inverter for Improved Harmonic Compensation Performance," *IEEE Transactions on Industrial Electronics*, vol. 62, pp. 40-51, 2015.

[10] J. C. Wu, H. L. Jou, Y. T. Feng, W. P. Hsu, M. S. Huang, and W. J. Hou, "Novel Circuit Topology for Three-Phase Active Power Filter," *IEEE Transactions on Power Delivery*, vol. 22, pp. 444-449, 2007.

[11] Z. Luo, M. Su, Y. Sun, W. Zhang, and Z. Lin, "Analysis and control of a reduced switch hybrid active power filter," *IET Power Electronics*, vol. 9, pp. 1416-1425, 2016.

[12] R. L. d. A. Ribeiro, T. d. O. A. Rocha, R. M. d. Sousa, E. C. d. Santos, and A. M. N. Lima, "A Robust DC-Link Voltage Control Strategy to Enhance the Performance of Shunt Active Power Filters Without Harmonic Detection Schemes," *IEEE Transactions on Industrial Electronics*, vol. 62, pp. 803-813, 2015.

[13] L. Wang, C. S. Lam, and M. C. Wong, "Unbalanced Control Strategy for A Thyristor-Controlled LC-Coupling Hybrid Active Power Filter in Three-Phase Three-Wire Systems," *IEEE Transactions on Power Electronics*, vol. 32, pp. 1056-1069, 2017.

[14] A. M. Al-Zamil and D. A. Torrey, "A passive series, active shunt filter for high power applications," *IEEE Transactions on Power Electronics*, vol. 16, pp. 101-109, 2001.

[15] A. Hamadi, S. Rahmani, and K. Al-Haddad, "A Hybrid Passive Filter Configuration for VAR Control and Harmonic Compensation," *IEEE Transactions on Industrial Electronics*, vol. 57, pp. 2419-2434, 2010.

[16] R. N. Beres, X. Wang, M. Liserre, F. Blaabjerg, and C. L. Bak, "A Review of Passive Power Filters for Three-Phase Grid-Connected Voltage-Source Converters," *IEEE Journal of Emerging and Selected Topics in Power Electronics*, vol. 4, pp. 54-69, 2016.

[17] V. F. Corasaniti, M. B. Barbieri, P. L. Arnera, and M. I. Valla, "Hybrid Power Filter to Enhance Power Quality in a Medium-Voltage Distribution Network," *IEEE Transactions on Industrial Electronics*, vol. 56, pp. 2885-2893, 2009.

[18] C. S. Lam, L. Wang, S. I. Ho, and M. C. Wong, "Adaptive Thyristor-Controlled LC-Hybrid Active Power Filter for Reactive Power and Current Harmonics Compensation With Switching Loss Reduction," *IEEE Transactions on Power Electronics*, vol. 32, pp. 7577-7590, 2017.

[19] C. S. Lam, W. H. Choi, M. C. Wong, and Y. D. Han, "Adaptive DC-Link Voltage-Controlled Hybrid Active Power Filters for Reactive Power Compensation," *IEEE Transactions on Power Electronics*, vol. 27, pp. 1758-1772, 2012.

[20] A. Bhattacharya, C. Chakraborty, and S. Bhattacharya, "Parallel-Connected Shunt Hybrid Active Power Filters Operating at Different Switching Frequencies for Improved Performance," *IEEE Transactions on Industrial Electronics*, vol. 59, pp. 4007-4019, 2012.

[21] S. Srianthumrong and H. Akagi, "A medium-voltage transformerless AC/DC power conversion system consisting of a diode rectifier and a shunt hybrid filter," *IEEE Transactions on Industry Applications*, vol. 39, pp. 874-882, 2003.

[22] H. Akagi, "Active Harmonic Filters," *Proceedings of the IEEE*, vol. 93, pp. 2128-2141, 2005.

[23] M. Wu, D. D. C. Lu, and C. K. Tse, "Direct and Optimal Linear Active Methods for Stabilization of LC Input Filters and DC/DC Converters Under Voltage Mode Control," *IEEE Journal on Emerging and Selected Topics in Circuits and Systems*, vol. 5, pp. 402-412, 2015.

[24] T. L. Lee, Y. C. Wang, J. C. Li, and J. M. Guerrero, "Hybrid Active Filter With Variable Conductance for Harmonic Resonance Suppression in Industrial Power Systems," *IEEE Transactions on Industrial Electronics*, vol. 62, pp. 746-756, 2015.

[25] C. Liu, B. Wu, N. R. Zargari, D. Xu, and J. Wang, "A Novel Three-Phase Three-Leg AC/AC Converter Using Nine IGBTs," *IEEE Transactions on Power Electronics*, vol. 24, pp. 1151-1160, 2009.

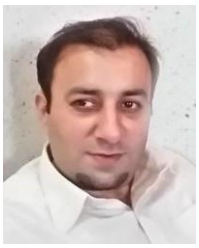

Wajahat Ullah Tareen (M'16) received the B.Sc. degree in electrical engineering from the University of Engineering and Technology, Peshawar, Pakistan, in 2007, and the master's degree from Brunel University, London, United Kingdom, in 2010. He is currently working toward the Ph.D. degree in the Power Electronics and Renewable Energy Research Laboratory, Department of Electrical Engineering, University of Malaya, Kuala Lumpur, Malaysia.

His research interests include Power Quality, power conversion techniques, UPS systems, and electric vehicles.

Saad Mekhilef (M'01, SM'12) received the B.Eng. degree in Electrical Engineering from University of Setif, in 1995, and Master of Engineering science and PhD from University of Malaya in 1998 and 2003 respectively. He is currently professor at Department of Electrical Engineering; University of Malaya. Prof. Saad is the author and co-author of more than 300 publications in international journals and proceedings. He is actively involved in industrial consultancy, for major corporations in the power electronics projects. His research interest includes power conversion techniques, control of power converters, renewable energy and energy efficiency.